Inorg. Chem. **2009**, *48*, 3296−3307

Forum

Structure and Magnetic Interactions in the Organic-Based Ferromagnet Decamethylferrocenium Tetracyanoethenide, $[FeCp^*_2]^{\bullet+}[TCNE]^{\bullet-}$

Jae-Hyuk Her,[†,⊥] Peter W. Stephens,[*,†] Jordi Ribas-Ariño,[‡] Juan J. Novoa,[*,‡] William W. Shum,[§] and Joel S. Miller[*,§]

Department of Physics & Astronomy, Stony Brook University, Stony Brook, New York 11794-3800, Department of Physical Chemistry and IQTCUB, University of Barcelona, Av. Diagonal 647, E-08028 Barcelona, Spain, and Department of Chemistry, University of Utah, Salt Lake City, Utah 84112-0850

Received September 1, 2008

The structures of three temperature-dependent polymorphs of solvent-free decamethylferrocenium tetracyanoethenide, $[FeCp^*_2][TCNE]$, are determined from high-resolution synchrotron powder diffraction data. $[FeCp^*_2][TCNE]$ is the first organic-based ferromagnetic material to be synthesized and is known to have two structural phase transitions at 249 and 282 K. The low-temperature phase, which exhibits spontaneous ferromagnetic order below 4.8 K, was determined at 12 K. At that temperature, it has monoclinic space group $P2_1/c$ [$a = 9.6637(4)$ Å, $b = 14.1217(5)$ Å, $c = 18.6256(7)$ Å, $\beta = 113.231(2)°$, $Z = 4$] and consists of parallel chains of alternating $[Fe(C_5Me_5)_2]^{\bullet+}$ and $[TCNE]^{\bullet-}$ ions, with an intrachain Fe···Fe distance of 10.45 Å. Structures of the intermediate and ambient temperature phases, also studied here, are characterized by increasing disorder. At 250 K, the unit cell space group is $P2_1/m$ [$a = 9.7100(3)$ Å, $b = 14.4926(4)$ Å, $c = 9.4997(3)$ Å, $\beta = 113.153(1)°$, $Z = 2$]. At ambient temperature, the lattice, albeit quite disordered, belongs to the orthorhombic space group $Cmcm$ [$a = 10.629(1)$ Å, $b = 16.128(1)$ Å, $c = 14.593(1)$ Å, $Z = 4$]. Nearest-neighbor magnetic interactions were evaluated for the 12 K structure by CASSCF and CASSCF/MCQDPT calculations (a methodology similar to the CASPT2 method). Similar trends are observed in computations with and without inclusion of spin−orbit coupling. The strongest are two intrachain $[FeCp^*_2]^{\bullet-}\cdots[TCNE]^{\bullet-}$ interactions (ferromagnetic with values of ∼45 and ∼29 cm^{-1}), although weaker, nonnegligible, ferro- or antiferromagnetic interchain interactions of less than ±0.2 cm^{-1} are also present. Magnetic interactions that lead to ordering are therefore three-dimensional, despite the vastly different intra- and interchain coupling strengths.

Introduction

The synthesis and magnetic characterization of decamethylferrocenium tetracyanoethenide, $[FeCp^*_2]^{\bullet+}[TCNE]^{\bullet-}$ ($T_c = 4.80$ K),[1,2] a score of years ago launched the field of organic-based magnets.[3] This electron-transfer salt has been the most extensively studied organic magnet and is a benchmark for comparison to other materials. The crystal structure of this material, particularly near T_c, is, however, unknown. In contrast, the magnetic properties are well characterized, the dominant spin coupling is ferromagnetic, as is evidenced by the fit of the temperature dependence of magnetic susceptibility in the paramagnetic phase, $\chi(T)$, to the Curie−Weiss expression, $\chi^{-1} \propto T - \theta$, and the observed $\theta > 0$ reflects ferromagnetic coupling. The molecular basis of magnetic interactions in this system has been discussed, with estimates for the exchange energy J derived from

* To whom correspondence should be addressed. E-mail: Peter.Stephens@sunysb.edu (P.W.S.), juan.novoa@ub.edu (J.J.N.), jsmiller@chem.utah.edu (J.S.M.).
[†] Stony Brook University.
[⊥] Current address: Department of Materials Science and Engineering, University of Maryland, College Park, MD 20742-2115, and NIST Center for Neutron Research, National Institute of Standard and Technology, Gaithersburg, MD 20899-6102.
[‡] University of Barcelona.
[§] University of Utah.

(1) (a) Miller, J. S.; Epstein, A. J.; Reiff, W. M. *Mol. Cryst., Liq. Cryst.* **1985**, *120*, 27. (b) Miller, J. S.; Calabrese, J. C.; Epstein, A. J.; Bigelow, R. W.; Zhang, J. H.; Reiff, W. M. *J. Chem. Soc., Chem. Commun.* **1986**, 1026. (c) Miller, J. S.; Calabrese, J. C.; Rommelmann, H.; Chittipeddi, S. R.; Zhang, J. H.; Reiff, W. M.; Epstein, A. J. *J. Am. Chem. Soc.* **1987**, *109*, 769. (d) Chittipeddi, S.; Cromack, K. R.; Miller, J. S.; Epstein, A. J. *Phys. Rev. Lett.* **1987**, *58*, 2695.

(2) Yeer, G. T.; Miller, J. S. In *Magnetism—Molecules to Materials*; Miller, J. S., Drillon, M., Eds.; Wiley-VCH: Mannheim, Germany, 2004; Vol. *5*, p 223. Gama, V.; Duarte, M. T. In *Magnetism—Molecules to Materials*; Miller, J. S., Drillon, M., Eds.; Wiley-VCH: Mannheim, Germany, 2004; Vol. *5*, p 1. Coronado, E.; Galàn-Mascarós, J. R.; Miller, J. S. *Compr. Organomet. Chem. III* **2006**, *12*, 413.

10.1021/ic801679m CCC: $40.75
Published on Web 04/13/2009

susceptibility and ordering temperature.[4] However, all such analyses, of this and other molecule-based magnets, have been made in the context of an assumed magnetic topology (the network of nonnegligible magnetic interactions among the radicals), which calls their validity into question.

In the present work, the molecular basis of magnetic interactions in this system is discussed based on estimates for the exchange parameters J_{AB} derived from accurate theoretical computations, a first-principles "bottom-up" methodology.[5] This allows us to determine the actual magnetic topology, which turns out to be three-dimensional in a way that cannot be fitted by any simple model. Thus, the relationship of macroscopic properties from the J_{AB} exchange parameters can only be determined using accurate numerical techniques.

When prepared from methyl cyanide (MeCN), the solvate $[FeCp^*_2]^{\bullet+}[TCNE]^{\bullet-}\cdot$MeCN forms, and its structure has been determined at 243 K.[1c] Its structure is composed of double sheets of parallel linear chains of alternating radical $[FeCp^*_2]^{\bullet+}$ cations (**C**) and radical $[TCNE]^{\bullet-}$ anions (**A**), which are in-registry within each sheet and out-of-registry with respect to adjacent sheets. The solvent forms layers that separate rows of these chains. The intrachain Fe···Fe separation is 10.415(2) Å.[1c] Attempts to determine the solvate structure at low temperature failed[1c] because of structural phase transitions that occur[6] and lead to the destruction of the crystals. Because of the facile loss of MeCN from the solvate, until recently[7] all of the physical studies, including the determination of T_c, were performed on solvent-free material, i.e., a phase different from the known crystal structure. Using excess solvent in equilibrium with the crystals, the magnetic behavior of solvated $[FeCp^*_2]^{\bullet+}$-$[TCNE]^{\bullet-}\cdot$MeCN was recently established, and it was found that the presence of the MeCN layers reduced T_c by 42% as well as substantially increasing the magnetic glassiness of the magnet.[7] This paper reports the crystal structure of solvent-free $[FeCp^*_2]^{\bullet+}[TCNE]^{\bullet-}$ prepared from the MeCN solvate.

Low-quality crystals of solvent-free $[FeCp^*_2]^{\bullet+}[TCNE]^{\bullet-}$ can be grown from tetrahydrofuran (THF). The room-temperature unit cell was determined to be orthorhombic, with an intrachain Fe···Fe separation of 10.621(2) Å.[1c] Evidently, the structure contains the same chains of alternating **A** and **C** radical ions as the MeCN solvate; however, because of severe disorder, the details of the structure could not be determined. Nonetheless, both the powder X-ray diffraction (PXRD) data and the magnetic studies[7] indicate that the structure of solvent-free $[FeCp^*_2][TCNE]$ made from THF is identical with that found for desolvated $[FeCp^*_2][TCNE]\cdot$MeCN. From an analysis of the temperature dependence of the specific heat, $C_p(T)$, the solvent-free phase was reported to undergo two structural phase transitions at 249 and 282 K,[6] again with destruction of the crystals upon cooling. The higher temperature peak in the $C_p(T)$ data is much broader and may actually be caused by two transitions. Hence, while $[FeCp^*_2]^{\bullet+}[TCNE]^{\bullet-}$ has been extensively studied and magnetically characterized,[1,2] its structure, especially near T_c, is unknown.

On the basis of a high-resolution powder diffraction study using synchrotron radiation, the temperature dependencies of the unit cell parameters and the Rietveld-refined structures of $[FeCp^*_2][TCNE]$ at 12, 250, and 295 K are reported. Using the structural parameters obtained at the lowest accessible temperature, 12 K, the magnetic interactions have been computed using the aforementioned first-principles bottom-up methodology.[5]

Experimental Details

Samples of $[FeCp^*_2]^{\bullet+}[TCNE]^{\bullet-}$ were made from MeCN as previously reported.[1c] Powder samples from THF were found to be significantly less crystalline and could not be used for structure determination. The samples were kept in an inert atmosphere until immediately prior to the diffraction studies. The crystallites had a needlelike morphology, and it was found that chopping them with a razor blade gave a satisfactory powder pattern, with minimum preferred orientations, whereas grinding degraded their crystallinity to the point that useful PXRD patterns for structure determination could not be obtained. Samples were flame-sealed into standard Lindemann glass capillaries and mounted in a closed-cycle He cryostat.

High-resolution PXRD patterns were collected at the X3B1 beamline of National Synchrotron Light Source, Brookhaven National Laboratory, at 12 K (base temperature) and 250 K and at X16C beamline at 295 K. A Si(111) double-crystal monochromator selected highly collimated incident beams of 0.69953(2) and 0.70162(1) Å, respectively, at the X3B1 and X16C beamlines. The diffracted X-rays after the sample were analyzed by a Ge(111) single-reflection crystal and detected using a NaI scintillation counter. The capillary was oscillated by 6° during data collection for better averaging of the powder pattern data. Besides full scans at 12 and 250 K, short scans of selected regions were collected at X3B1 beamline to identify changes in the lattice parameters and the phase transitions previously seen in specific heat measurements. *TOPAS-Academic* software was used to index, solve, and refine the crystal structure.[8−10]

Crystal Structure Results and Discussion

The full scan at 250 K can be indexed to monoclinic unit cell dimensions listed in Table 1. The 12 K scan contained a few extra peaks that could be indexed with the *c* axis

(3) Blundell, S. J.; Pratt, F. L. *J. Phys.: Condens. Matter* **2004**, *16*, R771. Ovcharenko, V. I.; Sagdeev, R. Z. *Russ. Chem. Rev.* **1999**, *68*, 345. Kinoshita, M. *Philos. Trans. R. Soc. London, Ser. A* **1999**, *357*, 2855. Miller, J. S.; Epstein, A. J. *Chem. Commun.* **1998**, 1319. Miller, J. S.; Epstein, A. J. *Chem. Eng. News* **1995**, *73#40*, 30. Miller, J. S.; Epstein, A. J. *Angew. Chem., Int. Ed. Engl.* **1994**, *33*, 385. Kinoshita, M. *Jpn. J. Appl. Phys.* **1994**, *33*, 5718. Gatteschi, D. *Adv. Mater.* **1994**, *6*, 635.

(4) Miller, J. S.; Epstein, A. J. *Angew. Chem., Int. Ed. Engl.* **1994**, *33*, 385–415.

(5) Deumal, M.; Bearpark, M. J.; Novoa, J. J.; Robb, M. A. *J. Phys. Chem. A* **2002**, *106*, 1299–1315.

(6) Nakano, M.; Sorai, M. *Mol. Cryst. Liq. Cryst.* **1993**, *233*, 161.

(7) Taliaferro, M. L.; Selby, T. D.; Miller, J. S. *Chem. Mater.* **2003**, *15*, 3602.

(8) Bruker AXS. *TOPAS V3: General profile and structure analysis software for powder diffraction data—User's Manual*; Bruker AXS: Karlsruhe, Germany, 2005.

(9) Coelho, A. A. *J. Appl. Crystallogr.* **2000**, *33*, 899.

(10) *TOPAS-Academic* is available at http://members.optusnet.com.au/alancoelho.

Table 1. Summary of the Crystallographic Parameters for [FeCp*$_2$][TCNE] at 12, 250, and 295 K

T (K)	12	250	295
a (Å)	9.6637(7)	9.7100(7)	10.629(1)
b (Å)	14.1217(10)	14.4926(10)	16.128(1)
c (Å)	18.6256(13)	9.4997(7)	14.593(1)
β (deg)	113.231(2)	113.153(1)	90
V (Å^3)	2335.7(5)	1229.16(3)	2501.6(5)
Z	4	2	4
space group	$P2_1/c$	$P2_1/m$	$Cmcm$
calcd density (g cm^{-3})	1.2922	1.2277	1.206
R_{wp} (%) [a]	4.2	4.736	5.198
GOF (R_{wp}/R_{exp})[b] = (reduced χ^2)$^{1/2}$	1.945	2.125	1.614

[a] The weighted profile R factor is defined as $R_{wp} = [\sum_i w_i(y_i^{calc} - y_i^{obs})^2/\sum_i w_i(y_i^{obs})^2]^{1/2}$, where y_i^{calc} and y_i^{obs} are the calculated and observed intensities at the ith point in the profile, normalized to the monitor intensity. The weight w_i is $1/\sigma^2$ from counting statistics, with the same normalization factor. N is the number of points in the measured profile. [b] The expected R factor is defined as $R_{exp} = [N/\sum_i w_i(y_i^{obs})^2]^{1/2}$.

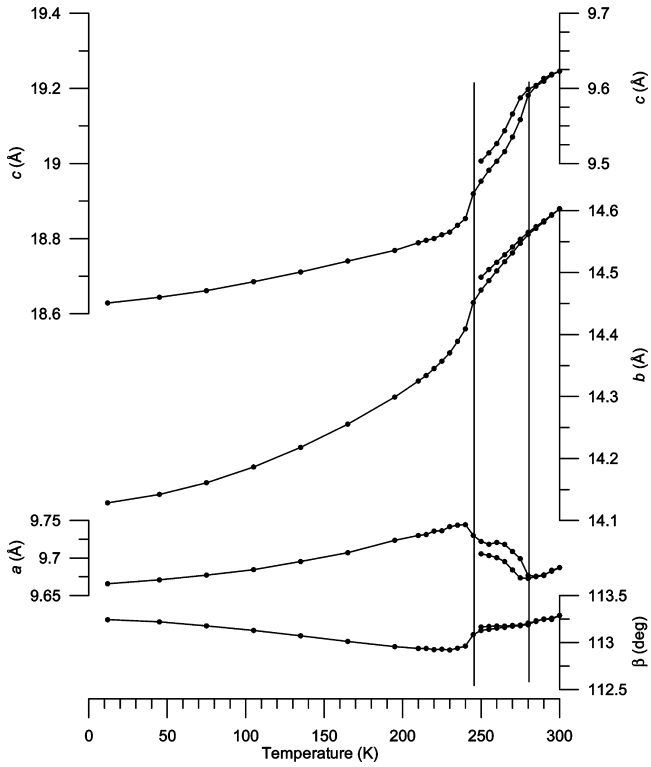

Figure 1. Temperature dependence of the monoclinic lattice parameters for [FeCp*$_2$]$^{\bullet+}$[TCNE]$^{\bullet-}$. The c scale at the left is for data below 245 K and at the right for data above 245 K. Data were collected upon heating from 12 to 300 K and then upon cooling to 250 K; note significant hysteresis in the range 245−280 K. Lines are drawn as guides to the eye; vertical lines at 245 and 280 K represent the most abrupt change in the lattice parameters but should not be taken as precise measurements of transition temperatures.

doubled. The previously observed room-temperature orthorhombic cell can be converted to similar monoclinic parameters (250 K) as $a_{mono} = c_{mono} = [a_{ortho}^2 + b_{ortho}^2]^{1/2}$, $b_{mono} = c_{ortho}$, and $\tan(\beta_{mono}/2) = b_{ortho}/a_{ortho}$. For temperatures ≥280 K, profile fits to the aforementioned low-angle data using monoclinic or orthorhombic cells are essentially indistinguishable.

In order to characterize the structural transitions known from heat capacity measurements,[6] the lattice parameters were determined between 12 and 300 K (Figure 1). The unit cell b and c lengths increase with increasing temperature; however, a is anomalous because it decreases with increasing temperature in the range 245−275 K. Changes in the lattice parameters are suggestive of two phase transitions in the neighborhood of 245 and 280 K, in accordance with the specific heat data. Within experimental resolution, the lattice parameters evolve continuously. Some degree of hysteresis is evident in the intermediate phase from the data collected on warming versus cooling; the second cooling curve was not followed into the low-temperature phase to see if it would close. The extra peaks due to the doubling of the c axis in the low-temperature phase are very weak as the temperature approaches 250 K; likewise, there is no clear signature of the monoclinic−orthorhombic transition near 280 K. Thus, accurate measurements of transition temperatures cannot be made from the diffraction data. It should be noted that neither of the phase changes has an associated magnetic anomaly,[1c] as would be expected for a change in the orientation that would lead to a change in the Landé g value.

To understand the structure of this system, particularly near the magnetic T_c, the structure was determined by direct-space-simulated annealing and Rietveld refinement of the high-resolution synchrotron powder diffraction data at 12 and 250 K. Systematic absences in the 250 K PXRD pattern (Figure 2, top) suggested space groups $P2_1$ or $P2_1/m$. The molecular volume implies $Z = 2$ formula units in the monoclinic cell, as either one formula unit in the irreducible cell of $P2_1$ or half a unit in $P2_1/m$. Rigid bodies, obtained from ref 1c, were used to describe the two molecular ions via z matrices in direct-space searches to determine the structure. Both ions could adopt a conformation with a mirror plane, but no solution could be found for the $P2_1/m$ space group with the ions on mirror planes. A candidate solution appeared in $P2_1$ with both ions in general positions. It was not possible to obtain an acceptable refinement of this model with any plausible distortion of the two ions and/or thermal parameters, and Fourier difference maps did not lead to any useful insights beyond the fact that there was substantial disorder. The best R_{wp} was 5.23% in space group $P2_1$; the resolution to this difficulty is discussed below.

The 12 K data (Figure 2, bottom) are very similar to those of the 250 K pattern but contain a few distinct additional peaks, which can be indexed if the c axis is doubled. Peaks ($h0l$) with l = odd are not observed, suggesting space group $P2_1/c$ with $Z = 4$. A total of 12 structural parameters were used in the simulated annealing solution: orientation and position of each of the molecular rigid bodies. Subsequently, the torsion angle between the two Cp* rings in the [FeCp*$_2$]$^{\bullet+}$ cation was allowed to refine, although the two Cp* rings were kept parallel on a common axis, bisected by the Fe atom. In the final refinement, atom positions were refined, retaining the idealized internal symmetries of the two molecular ions. H atoms were tethered to the methyl groups. Isotropic thermal parameters were held equal for all Cp* C atoms and for all TCNE atoms. The two Cp* rings are eclipsed, in contrast to the staggered configuration of the solvate. This result is strongly required by the data, with $R_{wp} = 4.20\%$ for the eclipsed configuration, versus 7.33% staggered with all other parameters varied.

Knowing the structure of the low-temperature phase, replacement of the c glide by a mirror plane is a very natural

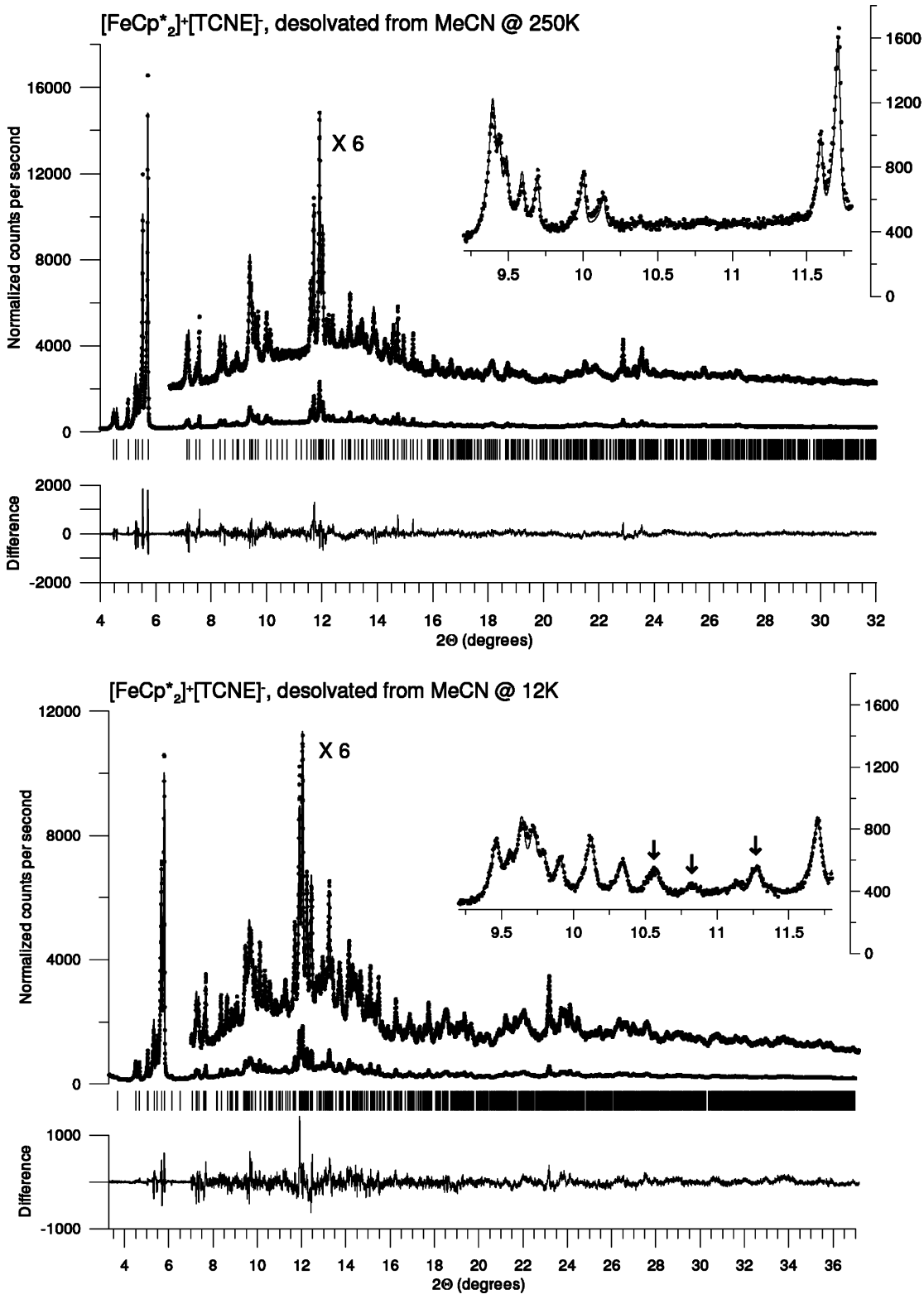

Figure 2. Rietveld fits of [FeCp*$_2$][TCNE] at 250 (top) and 12 K (bottom). The inset shows the part of the PXRD pattern where peaks from the doubled *c* axis are most visible.

suggestion of the structure of the 250 K phase. This reduces the *c* lattice parameter by half, to the value experimentally observed. Two different (superimposed) orientations of each molecule are then generated by the mirror plane in $P2_1/m$, which yields a significantly better refinement of the structure (Figure 2, top) with $R_{wp} = 4.74\%$ ($\chi^2 = 2.12$). Figure 3 shows the two structures in a manner that emphasizes their similarity. In this description, the 250 K structure is a disordered version of the 12 K structure. This is illustrated by the structure of [TCNE]$^{\bullet-}$ at 12 and 250 K (Figure 4a,b).

The room-temperature phase was previously described as orthorhombic with space group $Cmc2_1$.[1c] The $P2_1/m$ structure of the intermediate phase suggests that the room-temperature phase has *Cmcm* symmetry because it is a direct supergroup

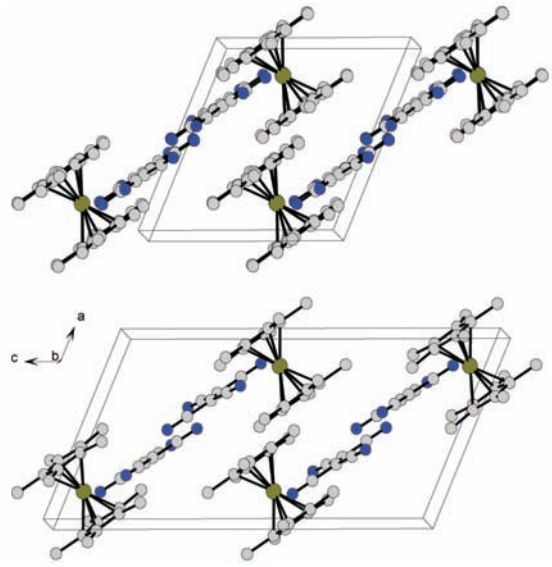

Figure 3. View of the monoclinic lattices of [FeCp*$_2$][TCNE] at 250 (top) and 12 K (bottom). Note the superposition of two different molecules in each location in the 250 K structure.

of $P2_1/m$ and has the same extinction class as $Cmc2_1$. Using the same techniques of simulated annealing with rigid molecules, followed by a Rietveld refinement, the structure was refined as shown in Figure 5. This solution has 4-fold disorder at each molecular position as a consequence of the general position having a multiplicity of 16, while the unit cell accommodates four formula units. The conversion from (intermediate-temperature) monoclinic to orthorhombic lattice vectors is given by

$$\begin{pmatrix} a_o \\ b_o \\ c_o \end{pmatrix} = \begin{pmatrix} 1 & 0 & 1 \\ 1 & 0 & -1 \\ 0 & 1 & 0 \end{pmatrix} \begin{pmatrix} a_m \\ b_m \\ c_m \end{pmatrix} \quad (1)$$

This shows that the monoclinic a and c axes must be equal in order that the phase be orthorhombic. In that case, $\tan(\beta_m/2) = b_o/a_o$. Those conditions are not enforced in the line-shape fits used to determine the lattice parameters near the transition shown in Figure 1. In the low-angle scans used to track the evolution of the lattice parameters with temperature, profile fits with enforced orthorhombic symmetry are essentially indistinguishable from monoclinic symmetry above 250 K, although the actual derived lattice parameters are slightly different.

Peaks in the orthorhombic phase with h and k both nonzero were observed to be significantly broader than others in the PXRD patterns. It was necessary to use extra line-shape parameters to account for this effect.[11] This suggests that the room-temperature phase, while having overall orthorhombic symmetry, contains local regions of monoclinic strain in which a_o and b_o are not perpendicular. The space group and location of the molecules are probably not uniquely defined by the data; there may be other equally satisfactory models incorporating a similar degree of disorder. However, the subgroup relationship (with appropriate changes in the lattice parameters) $Cmcm \supset P2_1/m \supset P2_1/c$ is compelling evidence for the description presented here.

Structure of [FeCp*$_2$][TCNE] at 12 K. The ordered, low-temperature phase of desolvated [FeCp*$_2$][TCNE] consists of chains of alternating donors and acceptors along the monoclinic [201] direction, with a repeating period of 20.89 Å.[12] If D, D′, A, and A′ denote the two orientations of donors and acceptors, the sequence along the chain is...DAD′A′.... Crystallographically, this is double the repeat distance of 10.415 Å in the MeCN solvate, [FeCp*$_2$][TCNE]·MeCN,[1c] because of the glide plane along the chain direction. However, the Fe−Fe distance of 10.451 Å is nearly identical with that of the solvate at 243 K (10.415 Å). Likewise, the donor−acceptor distances are very similar between the two structures; e.g., intrachain Fe−N distances range from 5.56 to 6.56 Å for [FeCp*$_2$][TCNE] vs from 5.628 to 6.471 Å for [FeCp*$_2$][TCNE]·MeCN.[1c]

The chains pack in a pseudotriangular lattice as shown in Figure 6. There are four distinct chains within each unit cell, related by the inversion centers and glide planes of the $P2_1/c$ lattice. The geometric relationships between neighboring molecules are illustrated in Figure 6, where center-to-center distances of all pairs of molecules of less than 10 Å are indicated. The geometry of neighboring molecular ions is required for the computation of magnetic interactions carried out below.

The lowest available temperature for the PXRD measurements was 12 K, significantly above the magnetic transition temperature. In an attempt to determine the accurate inter- and intramolecular separations at T_c, the unit cell was additionally refined at 20, 30, and 40 K, and computed intermolecular separations were plotted as a function of the temperature in order to extrapolate the distances to the value at the 4.8 K magnetic T_c. Within the estimated standard deviations, all of the distances were independent of the temperature; hence, the values at 12 K were used for computational studies (vide infra). There is, of course, the possibility of an additional structural distortion accompanying the magnetic transition, but given the weakness of the magnetic interactions, it is very unlikely.

Magnetic Interactions of [FeCp*$_2$]$^{\bullet+}$[TCNE]$^{\bullet-}$

Methodological Details. The strength and nature of the interaction between two spin-containing units can be characterized by the value of J_{AB} in the Heisenberg Hamiltonian ($\hat{H} = -2\sum_{A>B} J_{AB}\hat{S}_A\hat{S}_B$). Because both [FeCp*$_2$]$^{\bullet+}$ and [TCNE]$^{\bullet-}$ are doublets, values of J_{AB} for all symmetry-unique pairs of spin-containing units (A and B) were computed as $J_{AB} = [E(S)_{AB} - E(T)_{AB}]/2$, where $E(S)_{AB}$ and $E(T)_{AB}$ are the energies of the lowest-energy singlet and triplet states for the AB pair. The energies of these singlet and triplet states were computed by doing CASSCF and CASSCF/

(11) Stephens, P. W. *J. Appl. Crystallogr.* **1999**, *32*, 281.

(12) During the preparation of this manuscript, a single crystal of solvent-free [FeCp*$_2$]$^{\bullet+}$[TCNE]$^{\bullet-}$ at 100 K was obtained and its structure solved. That structure is in substantial agreement with the work cited herein. Gantzel, P.; Miller. J. S. Unpublished work.

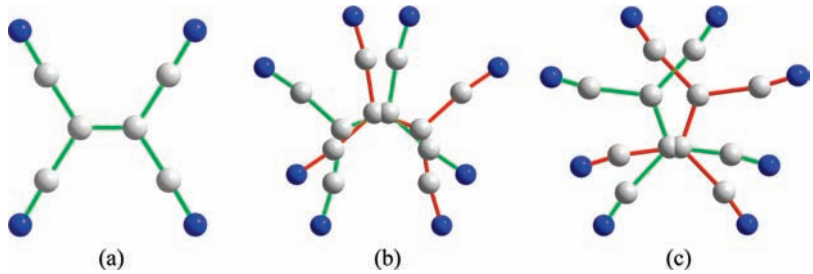

Figure 4. Refined structure of [TCNE]$^{\bullet-}$ at 12 (a), 250 K (b), and room temperature (c). In part b, each atom has a multiplicity of $^1/_2$ and in part c $^1/_4$.

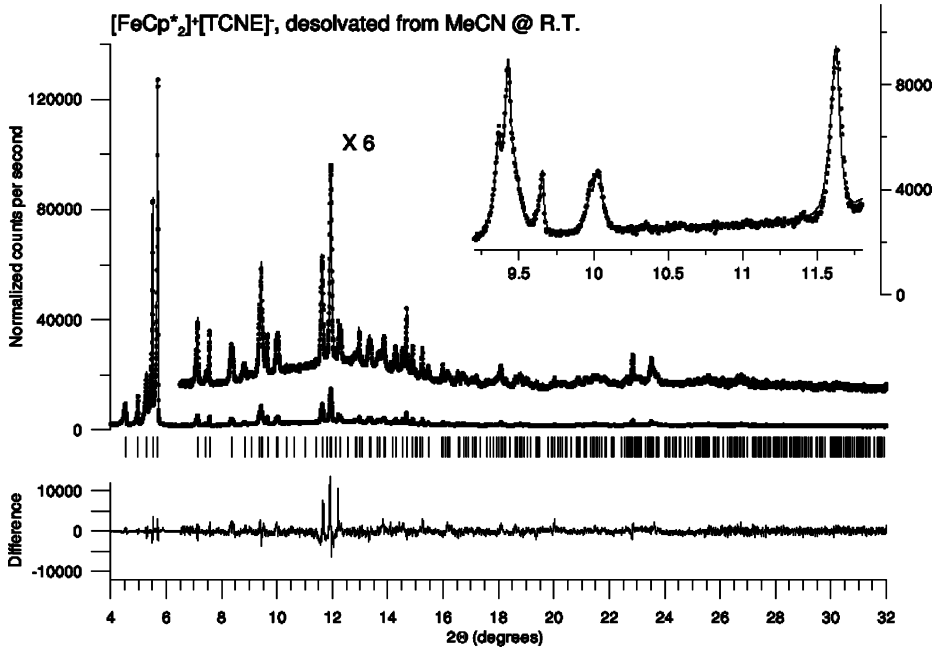

Figure 5. Rietveld refinement of [FeCp*$_2$][TCNE] at 295 K (room temperature).

Table 2. Geometric Relationship of All Unique Radical Pairs with Center-to-Center Distances ≤9 Å in the Structure of [FeCp*$_2$]$^{\bullet+}$[TCNE]$^{\bullet-}$[a]

	center-to-center distance, Å	nearest Fe−N distance, Å	other nearest distance, Å
		[FeCp*$_2$]$^{\bullet+}$···[TCNE]$^{\bullet-}$	
1	5.209	5.582	C−C[b] = 3.464
2	5.323	5.600	C−C[b] = 3.614
3	7.804	5.042	C−N = 3.576
4	8.278	5.311	C−N = 3.571
5	8.097	5.594	C−N = 3.712
8	7.408	5.563	C−N = 3.775
		[FeCp*$_2$]$^{\bullet+}$···[FeCp*$_2$]$^{\bullet+}$	
7	8.205		C−C[c] = 3.946
9	8.725		C−C[c] = 3.381
		[TCNE]$^{\bullet-}$···[TCNE]$^{\bullet-}$	
6	8.321		N−N = 3.408
10	8.662		N−N = 6.297

[a] Numbers **1**−**10** are identifiers used in the discussion of specific pairs. [b] Closest distance between the five-ring C atom of [FeCp*$_2$]$^{\bullet+}$ and the central C atom of [TCNE]$^{\bullet-}$. [c] Closest distance between methyl C atoms on neighboring [FeCp*$_2$]$^{\bullet+}$.

MCQDPT calculations using *GAMESS-06*[13] and the crystal geometry of each A−B pair. Depending on the structure of the A−B pairs, different (*n*, *m*) active spaces were employed on the CASSCF and CASSCF/MCQDPT calculations. Each active space was selected to allow a proper description of the electronic structure of the high and low spin states of the AB radical pairs and a similar quality among different A−B pairs. The [FeCp*$_2$]$^{\bullet+}$···[TCNE]$^{\bullet-}$ magnetic interactions were evaluated by CASSCF(8,7)/MCQDPT calculations[14] (that is, using an active space of eight electrons and seven orbitals). Note that there are two nearly degenerate singlets and two equally nearly degenerate triplets (Figure 7), which give rise to two nearly similar J_{AB} values (here, only the smallest one is reported). Because of their size (ca. 540 basis functions) and lack of symmetry, the [FeCp*$_2$]$^{\bullet+}$···[FeCp*$_2$]$^{\bullet+}$ magnetic interactions were com-

(13) Schmidt, M. W.; Baldridge, K. K.; Boatz, J. A.; Elbert, S. T.; Gordon, M. S.; Jensen, J. H.; Koseki, S.; Matsunaga, N.; Nguyen, K. A.; Su, S. J.; Windus, T. L.; Dupuis, M.; Montgomery, J. A. *J. Comput. Chem.* **1993**, *14*, 1347.

(14) The CASSCF/MCQDPT method performs a second-order perturbative calculation on a CASSCF multideterminantal wave function similar to that of the CASPT2 method, although using a different zeroth-order Hamiltonian in the perturbative expansion. Herein we used a CASSCF(8,7) wave function, obtained by allowing all possible combinations of eight electrons in seven orbitals [that is, using a (8,7) active space]. These orbitals include four Fe 3d orbitals (all but the Fe d_{z^2} orbitals, which test calculations using larger active spaces, have an occupation of 1.99 electrons, thus suggesting that it should be moved to the core orbitals), the two π occupied orbitals from each Cp fragment that can interact with the d_{xz} and d_{yz} orbitals of Fe and the SOMO of the TCNE fragment. The CASSCF wave functions of the two triplets and two singlets were obtained by two state-averaged CASSCF calculations, one for each state. The foundations of the CASSCF/MCQDPT method are described in: Nakano, H.; Nakayama, K.; Hirao, K.; Dupuis, M. *J. Chem. Phys.* **1997**, *106*, 4912.

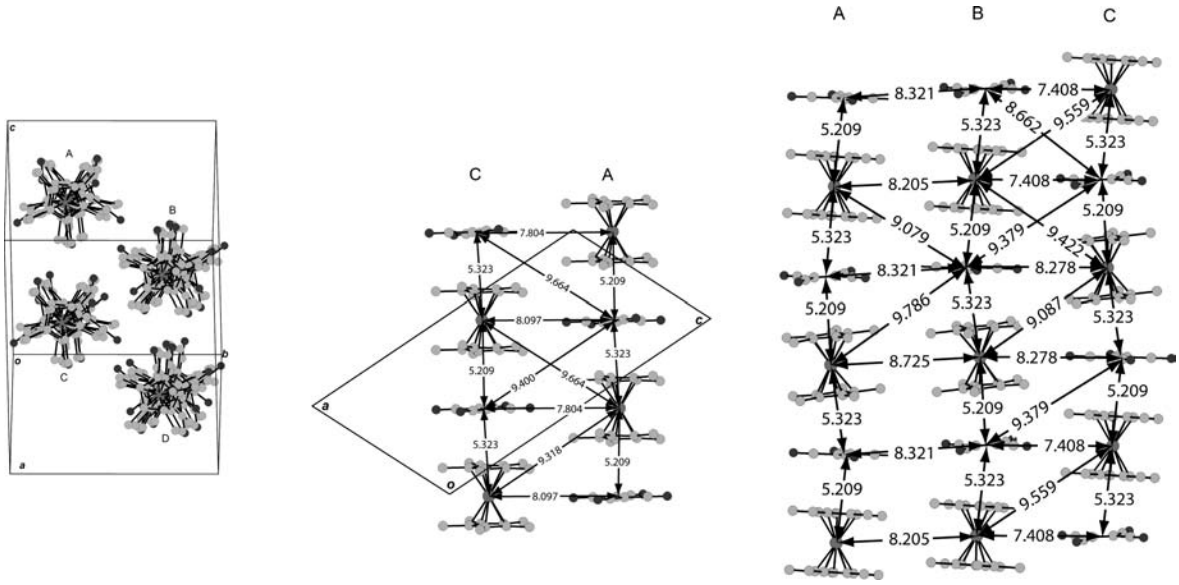

Figure 6. Packing of adjacent chains in the 12 K structure: (left) along the chains; (center and right) view perpendicular to the chains. Labels A−D denote chains related by lattice symmetry operations. Light lines in parts a and b represent the unit cell. Intermolecular distances are to the Fe atom in $[FeCp^*_2]^{\bullet+}$ and to the point between the two central C atoms in $[TCNE]^{\bullet-}$.

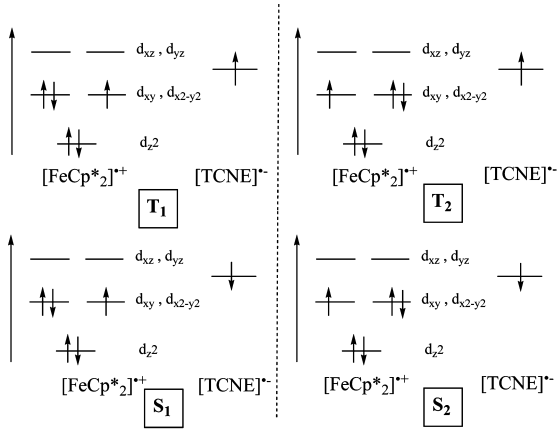

Figure 7. Schematic representation of the T_1 and T_2 triplet states and the S_1 and S_2 singlet states that arise from the magnetic interaction between a $[FeCp^*_2]^{\bullet+}$ cation and a $[TCNE]^{\bullet-}$ anion.

puted by doing only CASSCF(14,12) calculations. Finally, the $[TCNE]^{\bullet-}\cdots[TCNE]^{\bullet-}$ magnetic interactions were computed by doing CASSCF(2,2)/MCQDPT calculations; once CASSCF(6,6)/MCQDPT calculations on some of these radical pairs suggested that larger active spaces did not affect the J_{AB} value.[15] These calculations were done using Ahlrichs'[16] TZV basis set on Fe, the 6-31G basis set[16b] on all of the Cp ligands, and the 6-31+G basis set[16b] on the $[TCNE]^{\bullet-}$ anions. All J_{AB} interactions have been computed with an expected error smaller than ± 0.01 cm^{-1}.

The effect of the Madelung field of the crystal on the electronic structure of each AB pair was also taken into account in the computation of J_{AB}. This was done by surrounding each AB pair by their nearest ions (~1000 partial charges that include all $FeCp^*_2$ whose Fe···Fe distance with those of the central AB pair is less than 13.7 Å and also include all $[TCNE]^{\bullet-}$ whose N atoms are placed at less than 16 Å from the Fe atoms of the central $[FeCp^*_2]^{\bullet+}$) placed in a way that the local symmetry of the AB charge aggregates found is the same as the local ones found in the crystal and the sum of the net charges of the AB charge aggregates is zero (the net charge on each atom of the ions has been obtained by applying the Merz−Kollman procedure[17] on the B3LYP wave function for each isolated ion; these calculations were done using *Gaussian 03*[18] and the same basis set described above).

The spin−orbit coupling (SOC) effects play an essential role in the magnetic interactions associated with $[FeCp^*_2]^{\bullet+}$ because low-spin Fe^{III} has a nonquenched orbital angular momentum in its ground state. This is manifested in the value of g found for this radical ($g_\perp = 1.25$ to $g_\parallel = 4.4$).[19] Such a SOC can strongly affect the value of the energy of the high and low spin states and of the J_{AB} magnetic interaction in the $[FeCp^*_2]^{\bullet+}\cdots[TCNE]^{\bullet-}$ and $[FeCp^*_2]^{\bullet+}\cdots[FeCp^*_2]^{\bullet+}$ pairs. Therefore, besides reporting the J_{AB} values without SOC correction, the SOC-corrected J_{AB} values are also reported for these pairs by computing the SOC-corrected total energy for the high and low spin states. The SOC corrections on the CASSCF/MCQDPT-calculated J_{AB} values were done using the CASSCF wave function, and only the one-electron terms have been considered because inclusion of the two-electron terms (by modifying the nuclear charges in order to effectively account for these terms) does not change the values of the exchange coupling constants.[20] Within this approach, the SOC correction is done by computing and diagonalizing the matrix representation of the Hamiltonian

(15) CASSCF(6,6) calculations on one of the $[TCNE^-]_2$ dimers on the triplet give occupations for the six active orbitals of 1.93, 1.93, 1.00, 1.00, 0.07, and 0.07. These values indicate that a (2,2) space will give the same results. This is confirmed by computing the J_{AB} value: both active spaces give the value -0.16 cm^{-1}.

(16) (a) Schafer, A.; Huber, C.; Ahlrichs, R. *J. Chem. Phys.* **1994**, *100*, 5829. (b) Hehre, W. J.; Ditchfield, R.; Pople, J. A. *J. Chem. Phys.* **1972**, *56*, 2257.

(17) Besler, B. H., Jr.; Kollman, P. A. *J. Comput. Chem.* **1990**, *11*, 431.

(18) Frisch, M. J. et al.; *Gaussian 03*, revision C.02; Gaussian, Inc.: Wallingford, CT, 2004.

(19) Duggan, D. M.; Hendrickson, D. N. *Inorg. Chem.* **1975**, *14*, 955.

$\hat{H} = \hat{H}_O + \hat{H}_{SOC}$, the sum of spin-only and spin−orbit terms, computed on the basis of the states of interest. For each AB pair, the two lowest singlets ($M_s = 0$) and two lowest triplets ($M_s = -1, 0, 1$) were taken as the unperturbed states, so that $\hat{H}_O$ is a diagonal matrix whose eight elements are the CASSCF or CASSCF/MCQDPT energies of these states. $\hat{H}_{SOC}$ has zero diagonal elements, and its off-diagonal elements are the SOC terms evaluated using the CASSCF wave functions. The SOC corrections were only evaluated when the non-SOC-corrected J_{AB} values are nonnegligible (i.e., for $|J_{AB}| > 0.05$ cm^{-1}) and the SOC is expected to be relevant, that is, for the nonnegligible $[FeCp^*_2]^{\bullet+}\cdots[TCNE]^{\bullet-}$ radical pairs. (The $[FeCp^*_2]^{\bullet+}\cdots[FeCp^*_2]^{\bullet+}$ interactions are negligible, and the $[TCNE]^{\bullet-}\cdots[TCNE]^{\bullet-}$ interactions have no SOC.) There are eight SOC-coupled states arising from the linear combinations of the two triplet states ($M_s = -1, 0, 1$) and two singlet states ($M_s = 0$) depicted in Figure 7. After the SOC corrections were added and $\hat{H} = \hat{H}_O + \hat{H}_{SOC}$ was diagonalized, eight SOC-coupled states are obtained, which are separated into two groups with very different energies, of which only the four lowest ones can be thermally populated. Their energies cannot be fitted to an isotropic Heisenberg Hamiltonian as above, with only one isotropic J_{AB} value. However, assuming axial local symmetry, due to the C_5 rotation axis of $[FeCp^*_2]^{\bullet+}$, the four lowest-lying states can be fitted by the following anisotropic Heisenberg Hamiltonian: $\hat{H} = -2\sum_{A>B}(J_{AB\perp}\hat{S}_{Ax}\hat{S}_{Bx} + J_{AB\perp}\hat{S}_{Ay}\hat{S}_{By} + J_{AB\parallel}\hat{S}_{Az}\hat{S}_{Bz})$, where the isotropic J_{AB} has been substituted by $J_{AB\parallel}$ and $J_{AB\perp}$. Such a Hamiltonian is just a small variation from the Ising Hamiltonian (which contains only $J_{AB\parallel}$ terms) used sometimes in the literature[21] to describe SOC effects in coordination compounds.

Computation of the Magnetic Interactions in $[FeCp^*_2]^{\bullet+}[TCNE]^{\bullet-}$

The search for all unique radical−radical AB pairs present in the 12 K structure was done after analysis of the superstructure of the crystal, shown in Figure 6. We identified 20 pairs of molecules with center-to-center distances of less than 10 Å. (The center of $[FeCp^*_2]^{\bullet+}$ is the Fe atom, and that of $[TCNE]^{\bullet-}$ is a point midway between the central C atoms.) The center-to-center distance is not the most important parameter defining the magnetic interaction, but it is a convenient means to keep track of the geometric relationships. We confirmed that this list did not overlook any molecules whose atoms were close enough to touch (within van der Waals radii). We calculated isotropic J_{AB} values of all 20 pairs and found that it was negligible for all pairs with center-to-center distances greater than 9 Å. Pairs closer than 9 Å are listed in Table 2 and illustrated in Figure 8. While the center-to-center distance is convenient for bookkeeping, it is not particularly illuminating in considering the intermolecular magnetic interactions. In this system, the molecular orbitals about the Fe and N atoms are presumably more relevant. Table 2 also contains these nearest interatomic distances for each unique neighboring ion pair, as well as the closest intermolecular contacts as C−N distances between $[FeCp^*_2]^{\bullet+}$ and $[TCNE]^{\bullet-}$ pairs, and nearest C−C distances of $[FeCp^*_2]^{\bullet+}$ pairs. H atoms are not considered because their location is not really known from the PXRD measurements; in any event, it is not likely that the magnetically relevant orbitals have significant amplitude in the methyl groups.

The packing of cations and anions in the crystal is illustrated in Figure 9. Upon anticipation of the results of these computations, only the lines connecting pairs having nonnegligible magnetic interactions are shown there. The anion−cation chains illustrated in Figure 6, which are the shortest intermolecular distances, are seen as alternating red and dark blue lines.

All of the $[FeCp^*_2]^{\bullet+}\cdots[FeCp^*_2]^{\bullet+}$ radical pairs (**7**, **9**, and several others not specifically listed) have negligible isotropic J_{AB} values. There are four possible triplet states and four possible open-shell singlet states in these dimers. The four triplet configurations are shown in Figure 10; the four open-shell singlets are obtained from them by changing one spin-up electron to one spin-down electron. Closed-shell singlets are ionic states; as such, they can be neglected because they are much higher in energy than the four open-shell singlet and triplet states. These four open-shell singlet and triplet states become 16 states when the SOC is included. In these triplets, all of the singly occupied molecular orbitals (SOMOs) are degenerate, and thus, in a first approximation, all four triplets are expected to be degenerate. At the CASSCF(14,12) level, all of these states are nearly degenerate for all of the unique $[FeCp^*_2]^{\bullet+}\cdots[FeCp^*_2]^{\bullet+}$ pairs. Consequently, their isotropic J_{AB} is negligible ($\sim$0.00 cm^{-1}). The inclusion of the SOC does not lift the degeneracy, and thus the computed anisotropic $J_{AB\parallel}$ and $J_{AB\perp}$ values are also negligible.

The values of J_{AB} for the $[FeCp^*_2]^{\bullet+}\cdots[TCNE]^{\bullet-}$ **1**−**5** and **8** pairs, with and without the SOC correction, are presented in Tables 3 and 4, respectively. The isotropic J_{AB} values before the SOC corrections and the $J_{AB\parallel}$ and $J_{AB\perp}$ values after the SOC corrections are listed in Table 5. There is no single isotropic J_{AB} Hamiltonian that fits the whole energy spectrum of Table 3. However, the spectrum can be fitted using two isotropic $J_{AB}(i)$ parameters, one for each of the different types of symmetry to which the singlet and triplet states of Table 3 belong: $J_{AB}(1) = [E_S(1) - E_T(1)]/2$ and $J_{AB}(2) = [E_S(2) - E_T(2)]/2$. The fitting was done for the MCQDPT-calculated energies of Table 3, and the parameters of Table 5 were obtained. However, when the SOC correction was included, a good reproduction of the energy spectra for each radical pair (Table 4) was obtained with only two parameters using the following anisotropic Heisenberg Hamiltonian $\hat{H} = -2\sum_{A>B}(J_{AB\perp}\hat{S}_{Ax}\hat{S}_{Bx} + J_{AB\perp}\hat{S}_{Ay}\hat{S}_{By} + J_{AB\parallel}\hat{S}_{Az}\hat{S}_{Bz})$. The **1** and **2** intrachain pairs have the dominant magnetic interactions, with and without the SOC corrections, and both interactions

(20) Fedorov, D. G.; Koseki, S.; Schmidt, M. W.; Gordon, M. S. *Int. Rev. Phys. Chem.* **2003**, *22*, 551. It is known that the two-electron terms in a SOC calculation can be neglected provided that the nuclear charges in the one-electron term are replaced by effective nuclear charges. Abbeg, P. *Mol. Phys.* **1975**, *30*, 579. In these calculations, the effective charges for Fe, C, N, and H are 14.92, 3.60, 4.55, and 1.00, respectively. The validity of this one-electron approach was tested by also computing the two-electron terms (Tables S7 and S8 in the Supporting Information).

(21) Kahn, O. *Molecular Magnetism*; VCH: New York, 1993; p 261.

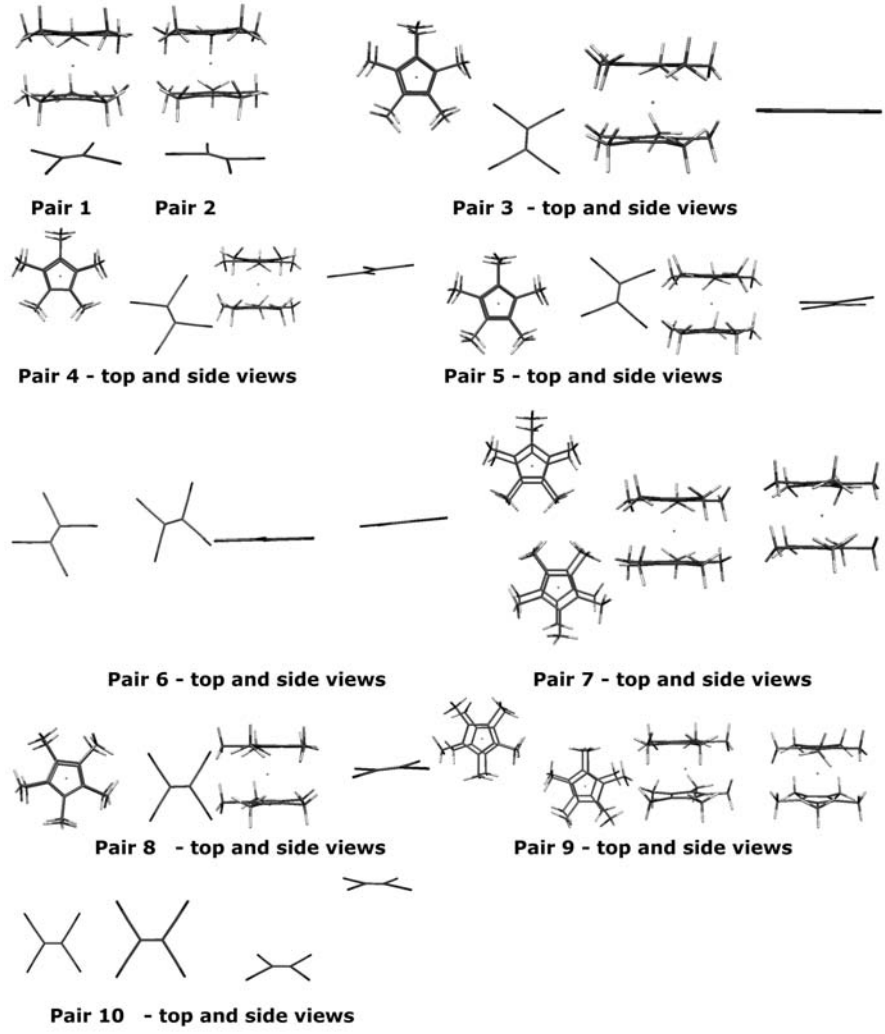

Figure 8. Illustrations of the $[FeCp^*_2]^{\bullet+}\cdots[TCNE]^{\bullet-}$, $[FeCp^*_2]^{\bullet+}\cdots[FeCp^*_2]^{\bullet+}$, and $[TCNE]^{\bullet-}\cdots[TCNE]^{\bullet-}$ pairs having center-to-center distances of less than 9 Å. Pair numbers are keyed to the entries in Table 2.

Table 3. Calculated CASSCF and MCQDPT Energies without the SOC Correction, for the T_1, T_2, S_1, and S_2 states for All Unique $[FeCp^*_2]^{\bullet+}\cdots[TCNE]^{\bullet-}$ Radical Pairs (**1**−**5** and **8**)

		energy[a] (cm^{-1})			
pair		$E(T_1)$	$E(T_2)$	$E(S_1)$	$E(S_2)$
1	CASSCF	0.0	17.31	53.34	71.07
	MCQDPT	0.0	40.15	90.51	133.82
2	CASSCF	0.0	8.50	33.84	39.28
	MCQDPT	0.0	21.34	55.85	68.54
3	CASSCF	0.0	26.99	0.17	27.15
	MCQDPT	0.0	54.52	0.34	54.84
4	CASSCF	0.0	7.05	−0.02	7.04
	MCQDPT	0.0	6.46	−0.07	6.39
5	CASSCF	0.0	22.64	0.0	22.65
	MCQDPT	0.0	54.47	0.0	54.48
8	CASSCF	0.0	31.72	−0.02	31.73
	MCQDPT	0.0	70.05	−0.09	70.04

[a] All of the energies are referred to the energy of the T_1 state.

are ferromagnetic. Nonnegligible magnetic interactions also exist between adjacent chains (pairs **3**−**5** and **8**, ferro- and antiferromagnetic in character). However, because these interactions are only a few times larger than the estimated numerical uncertainty, their relative error is much larger than the intrachain values. The three-dimensional network of nonnegligible ($|J_{AB}| > 0.05$ cm^{-1})[22] magnetic interactions generated in the crystal is shown in Figure 9. A comparison of Tables 2 and 5 reveals that the strength of the exchange interaction depends not only on the distance between neighboring atoms or molecules but also on their spatial relationships.

The J_{AB} isotropic coupling constants between the $[TCNE]^{\bullet-}\cdots[TCNE]^{\bullet-}$ pairs (**6**, **10**, and others >9 Å) were also computed (Table 6). In these radical pairs, there is only one triplet and one open-shell singlet state, and SOC corrections are not required in these pairs because no Fe atom is present. Only pair **6** has CASSCF(2,2) nonnegligible energies for both the T and S states, 0.00 and −0.16 cm^{-1}, respectively, in good agreement with the CASSCF(2,2)/MCQDPT values of 0.00 and −0.30 cm^{-1}. As mentioned above, this agrees with the CASSCF(6,6)/MCQDPT results. The computed CASSCF(2,2) and CASSCF(2,2)/MCQDPT for the isotropic J_{AB} value are −0.08 and −0.16 cm^{-1}, respectively. The resulting magnetic topology generated by **6** and $[TCNE]^{\bullet-}\cdots[TCNE]^{\bullet-}$ pairs is included in Figure 9. While pair **10** has a center-to-center distance only 0.34 Å

(22) Deumal, M.; Bearpark, M. I.; Robb, M. A.; Pontillon, Y.; Novoa, J. J. *Chem.—Eur. J.* **2004**, *10*, 6422.

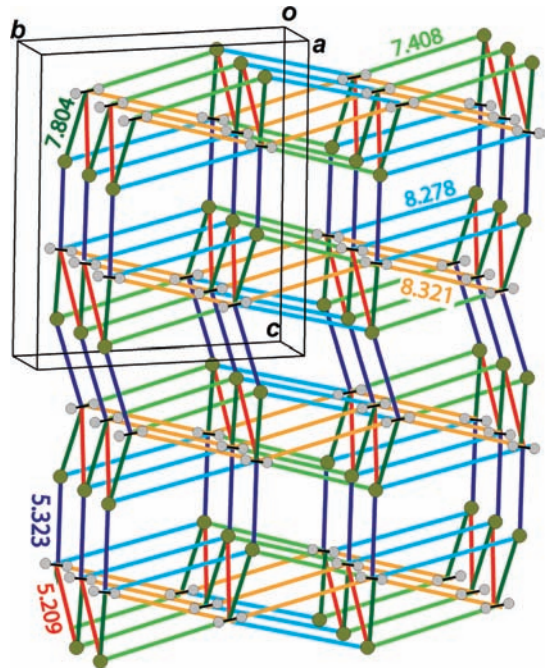

Figure 9. Simplified view of the superstructure of [FeCp*$_2$]$^{\bullet+}$[TCNE]$^{\bullet-}$ at 12 K. [FeCp*$_2$]$^{\bullet+}$ cations are represented by (green) Fe atoms, while the position of each [TCNE]$^{\bullet-}$ anion is represented by its two (gray) central C atoms and the bond between them. The network of magnetic interactions (the magnetic topology) among the radicals that created the most relevant [FeCp*$_2$]$^{\bullet+}$···[TCNE]$^{\bullet-}$ magnetic interactions are represented by colored lines as follows: red, **1**; dark blue, **2**; dark green, **3**; light blue, **4**; light green, **8**. The only significant [TCNE]$^{\bullet-}$···[TCNE]$^{\bullet-}$ interaction, from pair **6**, is shown in orange.

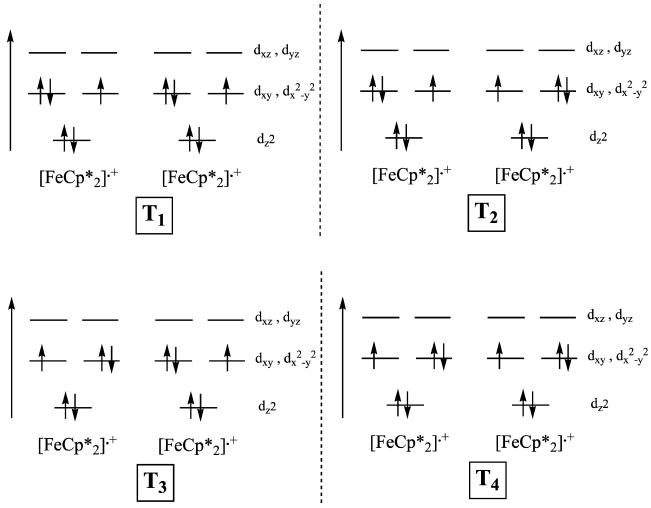

Figure 10. Schematic representation of the four possible triplet states that arise from the magnetic interaction between two [FeCp*$_2$]$^{\bullet+}$ cations. For each of these states, there is a corresponding open-shell singlet state that is obtained by converting one spin-up electron into one spin-down electron. Furthermore, there are eight closed-shell singlet states obtained by placing two electrons on the above half-filled orbitals not shown here because their energy is much higher for being ionic states.

greater than pair **6**, Table 2 and Figure 8 show that the relative orientation of pair **6** brings the N atoms of each molecule quite close together.

The total magnetic topology is that resulting from the various [FeCp*$_2$]$^{\bullet+}$···[TCNE]$^{\bullet-}$ and [TCNE]$^{\bullet-}$···[TCNE]$^{\bullet-}$ pairs. Clearly, the structural network has a three-dimensional topology; however, the interactions within a single chain are

Table 4. Calculated MCQDPT Energies with the SOC Correction Using the One-Electron Correction Terms Only, for the T_1, T_2, S_1, and S_2 States for All Unique [FeCp*$_2$]$^{\bullet+}$···[TCNE]$^{\bullet-}$ Radical Pairs (**1**−**5** and **8**)

SOC	state, energy,[a] cm^{-1}							
state	1	2	3	4	5	6	7	8
1	0.00	0.00	29.01	32.19	1385.93	1385.94	1416.55	1418.93
2	0.00	0.00	13.26	20.82	1385.42	1385.47	1399.39	1406.06
3	0.00	0.00	0.11	0.12	1385.75	1385.75	1385.86	1385.87
4	0.00	0.12	0.12	0.17	1384.77	1384.89	1384.89	1384.94
5	0.00	0.01	0.01	0.02	1385.28	1385.29	1385.29	1385.30
8	0.00	0.04	0.05	0.05	1386.47	1386.51	1386.51	1386.51

[a] These eight states are linear combinations of the two triplets (M_s = −1, 0, 1) and the two singlets (M_s = 0) (see the Supporting Information).

Table 5. Computed Isotropic, $J_{AB}(1)$ and $J_{AB}(2)$, and Anisotropic, $J_{AB\|}$ and $J_{AB\perp}$, Exchange Couplings for Exchange Coupling Energies of All Unique [FeCp*$_2$]$^{\bullet+}$···[TCNE]$^{\bullet-}$ Radical Pairs (**1**−**5** and **8**)[a]

pair	$J_{AB}(1)$, cm^{-1}	$J_{AB}(2)$, cm^{-1}	$J_{AB\|}$, cm^{-1}	$J_{AB\perp}$, cm^{-1}
1	+45.25	+46.84	+30.6	+1.6
2	+27.93	+23.60	+17.04	+3.78
3	+0.17	+0.16	+0.12	+0.01
4	−0.04	−0.03	−0.03	−0.08
5	0.00	+0.01	0.00	0.00
8	−0.05	−0.01	−0.03	−0.02

[a] The values of $J_{AB}(i)$ for each pair are (first and second columns) obtained from the MCQDPT energies of Table 3 using the equation $J_{AB}(i) = [E_S(i) - E_T(i)]/2$ and fit the isotropic Hamiltonian $\hat{H} = -2\sum_{A>B}[J_{AB}(1) + J_{AB}(2)]\hat{S}_A\hat{S}_B$. The values of $J_{AB\|}$ and $J_{AB\perp}$ for each pair (third and fourth columns) were computed by fitting the values of the MCQDPT energy spectra for the pair to the anisotropic Hamiltonian $\hat{H} = -2\sum_{A>B}(J_{AB\perp}\hat{S}_{Ax}\hat{S}_{Bx} + J_{AB\perp}\hat{S}_{Ay}\hat{S}_{By} + J_{AB\|}\hat{S}_{Az}\hat{S}_{Bz})$.

Table 6. Calculated CASSCF and CASSCF/MCQDPT Energies (First and Second Rows within Each Radical, Respectively) for the T_1 and S_1 States for All Unique [TCNE]$^{\bullet-}$···[TCNE]$^{\bullet-}$ Relevant Pairs

		energy (cm^{-1})	
pair		$E(T_1)$	$E(S_1)$
6	CASSCF	0.0	−0.16
	MCQDPT	0.0	−0.30
10	CASSCF	0.0	0.0
	MCQDPT	0.0	0.0

much stronger than those between chains. Likewise, a three-dimensional topology remains from a consideration of $J_{AB\|}$,and $J_{AB\perp}$ SOC-corrected results because (a) the $J_{AB\perp}$ component is always very small (the Heisenberg Hamiltonian is reduced to an Ising Hamiltonian because of the SOC effect) and (b) the $J_{AB\|}$ values are reduced by a similar percentage with respect to their isotropic J_{AB} counterparts. Hence, the magnetic interactions are dominated by the ferromagnetically coupled intrachain J_{AB}(**1**) and J_{AB}(**2**). Interchain interaction **3** is also ferromagnetic, so the chains are coupled into (101) sheets. The interactions **4**, **6**, and **8**, between the (101) sheets, are all antiferromagnetic. Hence, inclusion of SOC does not affect (1) the order of magnitude of the magnetic interactions, (2) their relative strength, or (3) the strong anisotropy of the magnetic interactions.

Finally, we discuss the nature of the dominant magnetic interaction, J_{AB}(**1**). CASSCF(8,7)/MCQDPT calculations indicate that this is ferromagnetic; i.e., it has a triplet ground state. The CASSCF(8,7) wave function has three SOMOs, with occupation 1.5, 1.5, and 1.0; these orbitals are illustrated in Figure 11. All other orbitals have occupations close to 2.0 or 0.0. The two SOMOs with occupation 1.5 correspond to nonbonding d_{xy} and $d_{x^2-y^2}$ orbitals of Fe, while the SOMO with occupation 1.0 corresponds to the bonding combination

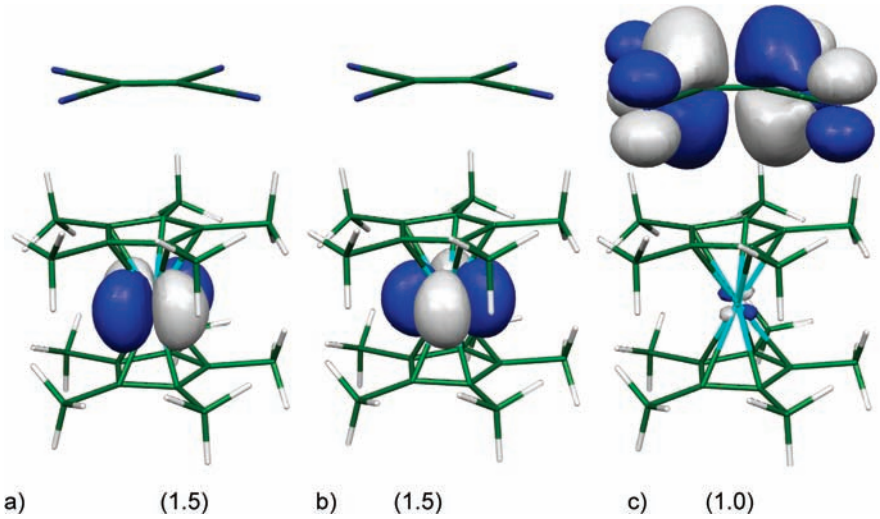

Figure 11. Shape of the three SOMO orbitals in the CASSCF(8,7) wave function for the triplet ground state (these three orbitals are the only ones among the active orbitals having occupations far from 2.0 or 0.0). Populations are indicated under each orbital.

between the π^* orbital of $[TCNE]^{\bullet-}$ and the d_{xz} orbital of Fe. This confirms the qualitative diagram of Figure 7, with the two triplet states carrying approximately equal weight. In the $\pi^*[TCNE]^{\bullet-} + d_{xz}(Fe)$ orbital, the dominant component is $\pi^*[TCNE]^{\bullet-}$ by 80%. This orbital also has a small but significant component on the C atoms of the Cp* rings (not visible in the figure because of its small weight in that region), but no component is observed on the H atoms of $[FeCp^*_2]^{\bullet+}$. Note that a [1.5, 1.5, 1.0] occupation is typical for a multireference wave function, where two configurations in which the three SOMOs of Figure 11 have occupations [2, 1, 1] and [1, 2, 1] are combined with a 50% weight. These results allow us to conclude that the main driving force for the magnetic interaction of pair **1** is associated with the overlap of $\pi^*[TCNE]^{\bullet-}$ and $d_{xz}(Fe)$ orbitals (Figure 11c), which results in a SOMO in pair **1** that is nearly orthogonal by symmetry to the partially occupied Fe e_g (d_{xy} and $d_{x^2-y^2}$) orbitals, thereby explaining the triplet ground state of this dimer. This description only points at the main component of the interaction leading to magnetic ordering. Other overlaps are also possible among the $[FeCp^*_2]^{\bullet+}$ and $[TCNE]^{\bullet-}$ orbitals of the same symmetry, but their contribution is minor.

Conclusion

While $[FeCp^*_2]^{\bullet+}[TCNE]^{\bullet-}$ was synthesized more than 20 years ago, the crystal structure of that first molecule-based magnet has been unknown in detail until this work. Not surprisingly, the structure is closely related to the solvate $[FeCp^*_2]^{\bullet+}[TCNE]^{\bullet-}\cdot MeCN$, and the factor of 2 difference in magnetic transition temperatures apparently stems from rather subtle changes in the geometry. The two features previously observed in specific heat have been identified as successive crystallographic order−disorder transitions. Knowledge of the crystal structure of the magnetic phase permits a detailed analysis of the magnetic interactions in this material.

The computed results indicate that there is a quite strong intrachain ferromagnetic coupling ($J_{AB} > 0$) between the $[FeCp^*_2]^{\bullet+}$ cations and $[TCNE]^{\bullet-}$, which agrees with the experimental data available. The magnetic behavior of the chains, however, cannot be described by only one J_{AB} coupling between $[FeCp^*_2]^{\bullet+}$ and $[TCNE]^{\bullet-}$, but two different J_{AB} parameters are needed in order to properly describe the magnetic behavior between cations and anions within a chain.

In contrast, the interchain interactions are both ferro- ($J_{AB} > 0$) and antiferromagnetic ($J_{AB} < 0$) between specific $[FeCp^*_2]^{\bullet+}$ cations and the $[TCNE]^{\bullet-}$ anions. It must be noted that the computed magnitudes of some of these interactions are only a few times larger than their estimated uncertainties. The only ferromagnetic pathway between chains (which is the strongest one in absolute value) found is associated with pair **3**. The ferromagnetic planes, in turn, are weakly antiferromagnetically coupled via the **4**, **6**, and **8** interaction pathways. Therefore, the interchain exchange interactions between $[FeCp^*_2]^{\bullet+}$ and $[TCNE]^{\bullet-}$ cannot account by themselves for the three-dimensional ferromagnetic ordering of the $[FeCp^*_2][TCNE]$ bulk magnet. To explain the bulk magnetic behavior, magnetic dipolar interactions may play an additional, but essential, contribution. Magnetic dipolar interactions should have magnitude similar to the extremely low values of some of the antiferromagnetic interchain J_{AB} values, but their cooperative nature could strengthen their relevance. The inclusion of the SOC in the J_{AB} values does not modify the magnitude or relative strength of the J_{AB} in different pairs or the magnetic topology, a three-dimensional topology with dominant ferromagnetic interactions. The main change introduced by the SOC effect is the presence of a magnetic anisotropy that was not present when no SOC corrections are made.

Acknowledgment. We are grateful for useful discussions with Alan Coelho and samples prepared by Michelle L. Taliaferro. We acknowledge continued partial support from the U.S. Department of Energy (No. DE FG 03-93ER45504) and the AFOSR (No. F49620-03-1-0175). The National Synchrotron Light Source, Brookhaven National Laboratory,

was supported by the U.S. DOE, Office of Basic Energy Sciences, under Contract DE-AC02-98CH10886. J.S.M. appreciates the support of the Catalan Autonomous Government (Contract 2003PIVB 00079) for a Visiting Professorship that made a sabbatical stay in Barcelona possible. J.R.-A. and J.J.N. acknowledge the allocation of computer time by CESCA/CEPBA and support from the Spanish Science and Education Ministry (Nos. CTQ2005-02329 and UNBA05-33-001) and the Catalan Autonomous Government (Nos. 2005SGR-00036 and 2005 PEIR 0051/69). J.R.-A. also thanks the Spanish Science and Education Ministry for his Ph.D. grant.

Supporting Information Available: Crystallographic data (atomic positions, thermal parameters, bond lengths, raw powder diffraction data, and fitted profiles) for [FeCp*$_2$][TCNE] at 295, 250, and 12 K in the form of CIF files, possible network of magnetic J_{AB} interactions, SOC wave functions, calculated MCQDPT energies, and computed anisotropic exchange couplings. This material is available free of charge via the Internet at http://pubs.acs.org. The atomic coordinates for these structures have been deposited as CCDC 700811−700813, respectively, with the Cambridge Crystallographic Data Centre. The coordinates can be obtained, upon request, from the Director, Cambridge Crystallographic Data Centre, 12 Union Road, Cambridge CB2 1EZ, U.K.

IC801679M